Spatio-temporal analysis of an electrophysiological wave phenomenon *

Edmond Jonckheere and Poonsuk Lohsoonthorn
Department of Electrical Engineering -Systems
University of Southern California
Los Angeles, CA 90089-2563
jonckhee@usc.edu lohsoont@hotmail.com

Abstract

An electrophysiological phenomenon running along the spine, referred to as Network Spinal Analysis (NSA) wave, is analyzed from the "inverse" viewpoint of constructing the traveling and stationary wave phenomena from the surface electromyographic (sEMG) signals recorded at various points along the paraspinal muscles. Statistical correlation techniques are used to identify the propagation delay and phase shift of the phenomenon from one point to another along the spine. Since the sEMG signals consist of a great many "bursts," the wave is most easily detected from some specific subband signals of the Daubechies wavelet decomposition. As a therapeutic application, it is shown that partial recovery from spinal cord injury can be assessed by the correlation between the sEMG signals on both sides of the injury. More fundamentally, for a quadriplegic subject who has had some recovery, the wave appears to travel through the injury area, but does not quite settle in a stationary pattern as it would be in a normal subject.

1 Introduction

In a book [2] that has captured the attention of spine health professionals, the Scandinavian neurosurgeon Alf Breig introduced the concept of *Adverse Mechanical Tensions in the Central Nervous System*. The tenet of this theory is the fact that, at the cranial level, the dura mater of the spinal cord is mechanically attached to the circumference of the foramen magnum and, at the basin level, the cord is attached to the coccyx via the filum terminale. Under flexion and extension, the length of the cord changes considerably and hence the cord is subject to mechanical tensions, which become pathological, and hence impair

*The research, which involves human subjects, was approved by the Institutional Review Board (IRB) of the University of Southern California and was supported by the Association for Network Care.

nerve activity, in case the movement of the cord is restricted by space-occupying lesions or scar tissue. It has been argued by Breig that some diseases (including multiple sclerosis [2, p. 177]) have this neuro-biomechanical origin and that relieve of these adverse tensions could alleviate symptoms [3].

In addition to the attachment of the dura to the ring of the atlas, there is also evidence [15] of direct attachments of the dura to the osseous structures of the vertebra at the C2-C6 levels, although it seems that there is considerable variation among individuals.

Other sources of pathological tensions besides those already mentioned include vertebral misalignment or postural problems. Pathological tensions in the spinal cord induce hyperstimulation of the proprioceptive fibers afferent to the spine, resulting in impaired functionality of the spine at the attachment level and other effects at other parts of the nervous system.

More closely related to the present paper is the fact that dural attachments appear to create extra feedback paths from the mechanical movement of the spine to the Central Nervous System (CNS). In the motor reflex loop, the degree of stretch of the paraspinal muscles is recorded by the neuromuscular spindles and transmitted by afferent fibers to the motor neurons in the spine, back to the muscles via the efferent fibers [11, p. 41, 139]. However, the dural attachment creates an extra feedback path from the paraspinal muscles *directly* to the spinal neurons. The existence of this extra feedback path[1] is probably what makes the spinal oscillators, the existence of which has been demonstrated by a technique referred to as *Network Spinal Analysis*^{TM} *(NSA) care*. In this technique, the practitioner locates the Spinal Gateway^{TM} area, which is on the skin overlying or in the vicinity of the dural-vertebral attachments, based on his (her) professional assessment of the status of the active, passive, and neural subsystems supporting the normal function of the nervous system [10], and sensitizes the areas to the point where a slight pressure at the spinal gateway area elicits an oscillation that takes, initially, the form of a slight muscular movement or localized twitch in the neck area.

Likewise, an oscillation can also be triggered at the sacral level, where the feedback mechanism is provided by the attachment of the *filum terminale*, the distal end of the spine, to the coccyx.

The cervical, sacral oscillators create waves propagating downward, upward, respectively, along the spine, until they take the external appearance of a spontaneous, involuntarily controlled rocking motion of the spine, referred to as NSA wave. As the care progresses through a series of levels of care, the NSA wave itself both visually and mathematically [8, 7] undergoes significant changes. The NSA wave produces a rather intensive exercise for the spine and the back musculature, not reproducible by any other physiotherapeutical means. This has also been claimed to relieve *adverse mechanical tensions* in the cord. More closely related to the present paper is the fact that this involuntary physical activity is of the same kind as the repetitive activity that has shown therapeu-

[1] As pointed to us by Mr. Vikram Mahajan, there is also possibly a disturbance of the inhibitory pathways involved.

tic benefits for a five years post injury quadriplegic patient [9]. In fact, as the study of Section 4 demonstrates, another quadriplegic patient with a similar injury recovered some sensory and motor functions after NSA care. One can only speculate that, for a patient with a spinal injury around C4, the nervous activity generated by the cervical and sacral oscillators *on both sides of the spine injury* reconstructs, through Hebb's law, synaptic strengths in the periphery of the injury, thereby achieving some "rewiring."

The purpose of this paper is, first, to positively establish the traveling and stationary wave phenomena between the neck and the sacrum during NSA care and, second, to use the wave properties to asses the amount of motor recovery in spinal injury patients.

The proposed technique to positively demonstrate existence of the wave is basically to establish that the voltage signal at one place along the spine, referred to as surface Electromyographic (sEMG) signal, is statistically correlated with the time-shifted versions of other signals recorded at other points along the spine. In the first, traveling wave, analysis (Section 2.1), the mutual information between a signal at one point and the time-shifted signal at another point is investigated. The delay achieving maximum mutual information is the time it takes for the wave to travel from one point of sEMG recording to the other. In the second, stationary wave, analysis (Section 2.2), the correlation among the sEMG phenomena along the spine is shown to provide a phase shift and is hence used to construct the "mode shape," typical of a stationary wave.

The problem is that the sEMG signal consists, notwithstanding various noise, of many "bursts" running up and down the spine. As such, statistical correlation analysis on the raw signals only establishes a *traveling* wave phenomenon, easily visualized by "following the burst." To detect a coherent *stationary* wave phenomenon, it is necessary to restrict ourselves to some relevant component of the signal, which is most easily identified as a selected subband of the Daubechies DB_3 wavelet decomposition (Section 2.2.2). Besides, the same wavelet decomposition allows some preprocessing: The signal during NSA care is wavelet decomposed and compared with the wavelet decomposition of a control signal recorded when the wave phenomenon was absent. This indicates that only part of the wavelet decomposition was really relevant to the NSA wave phenomenon.

2 Spatio-temporal analysis of signals

Here, we develop the so-called *spatio-temporal technique,* the aim of which is to positively identify a wave phenomenon from the analysis of the signals recorded at several points along the spine.

The first analysis (Section 2.1) is the *canonical correlation* of the past sEMG process at some point along the spine and the time-shifted future sEMG process at another point. Quantitatively, the analysis proceeds via the singular values to the *mutual information* between the past of the process at one point and the future of the time-shifted process at the other point. The rationale is quite simple: Should there be a need of a time-shift to observe a maximum mutual

information, then it can be argued that there is a wave traveling *from* the first point *to* the second point. In fact the first point can be identified as the "cause" while the second point is identified as the "effect."

The second analysis (Section 2.2) is computationally simplified by treating the sEMG phenomena at the 4 points along the spine as a collection of 4 random variables. It relies on the correlation analysis of one random variable with the time-shifted version of the random variable at another point. The advantage of this new method is that the correlation provides the cosine of the phase angle between the signal at one point and the time-shifted version of the signal at the other point. As such, a consistent phase pattern with "zero crossing nodes" would reveal a *stationary* wave phenomenon and would in fact give some clues about the mode shape.

2.1 Canonical correlation among time-shifted signals at various points

The time-shifted linear canonical correlation analysis proceeds as follows: Let T_s be the time-shift and L be the "lag," that is, the order of the model that would result from this analysis. Let $X(k)$ and $Y(k)$ be the sEMG signals at two points along the spine. Then the past observation of the (zero-mean) process X at time k is

$$X_{-}(k) = \left(X(k), \ldots, X(k-L+1)\right)^{T}$$

and the future observation of the (zero-mean) process Y at time k is

$$Y_{+}(k) = \left(Y(k+1), \ldots, Y(k+L)\right)^{T}$$

The canonical correlation matrix between the (zero-mean) processes $X_{-}(k)$ and $Y_{+}(k+T_s)$ is

$$\Gamma(T_s) = \left(EX_{-}(k)X_{-}^{T}(k)\right)^{-1/2}\left(EX_{-}(k)Y_{+}^{T}(k+T_s)\right)\left(EY_{+}(k+T_s)Y_{+}^{T}(k+T_s)\right)^{-1/2}$$

where $Q^{-1/2}$ denotes the inverse of the Cholesky factor or symmetric square root of $Q = Q^{T} > 0$. This matrix can be singular value decomposed as

$$\Gamma(T_s) = U(T_s)\,\Sigma(T_s)\,V(T_s)$$

where $U(T_s)$ and $V(T_s)$ are orthonormal matrices and $\Sigma(T_s)$ is a diagonal matrix of $\sigma_i \in [0,1], i = 1, ..., L$, called time-shifted *canonical correlation coefficients*.

This approach is statistically implemented as follows: Define the crosscorrelation between the past observation of the process X and the future observation of the process Y, time shifted by T_s, to be the $L \times L$ matrix

$$C_{X_{-}Y_{+}}(T_s) = \frac{1}{K-2L+1}\sum_{k=L}^{K-L-T_s} X_{-}(k)^{T}\,Y_{+}(k+T_s)$$

Define the autocorrelation of past observation as

$$C_{X_-X_-} = \frac{1}{K-L+1}\sum_{k=L}^{K} X_-(k)^T X_-(k)$$

and the autocorrelation of the future observation as

$$C_{Y_+Y_+} = \frac{1}{K-L+1}\sum_{k=0}^{K-L} Y_+(k)^T Y_+(k)$$

Define the Cholesky decompositions of $C_{X_-X_-}$ and $C_{Y_+Y_+}$ as

$$\begin{aligned} C_{X_-X_-} &= T_{X_-}^T T_{X_-} \\ C_{Y_+Y_+} &= T_{Y_+}^T T_{Y_+} \end{aligned}$$

where T_{X_-} and T_{Y_+} are lower triangular matrices. The canonical correlation matrix with time-shift T_s is estimated as

$$C(T_s) = T_{X_-}^{-T} C_{X_-Y_+}(T_s)\, T_{Y_+}^{-T}$$

The singular values of the above matrix are collected in decreasing order along the diagonal of another matrix denoted as $S(T_s)$. The predictability of the future of the time-shifted sequence Y given the past of the sequence X is characterized by the past/future mutual information

$$I_{XY}(T_s) = -\frac{1}{2}\log\det\left(I - S(T_s)^2\right)$$

where I is the identity $L \times L$ matrix. Define the optimal time shift T_s^* as follows:

$$T_s^* = \arg\max_{0<T_s\leq K} I_{XY}(T_s)$$

Existence of some mutual information between $X_-(k)$ and $Y_+(k+T_s)$ indicates existence of a regression relation that could take either form:

$$\begin{aligned} Y_+(k+T_s) &= AX_-(k) + b \\ X_-(k) &= A'Y_+(k+T_s) + b' \end{aligned}$$

The first one is usually referred to as construction of the state over the past while the second one is construction of the state over the future. Which regression should be preferred depends on the behavior of the mutual information I_{XY} with T_s. On the raw signal, it was found that $T_s^* > 0$, so that this parameter can be interpreted as the propagation delay of some wave along the spine traveling from the point of observation of X to the point of observation of Y. In other words, X is the cause and Y is the effect, Y is the delayed response to X, and the first regression should be preferred. Clearly, this analysis would yield a dynamical model of Y driven by the "excitation" X.

We conjecture that this situation would typically happen if X is observed at the point along the spine where the practitioner applies pressure and Y is observed at another point along the spine.

Remark: The chief difference between the above-described analysis and the previous one reported in [1] is that, in the previous one, we did the canonical correlation analysis of the past and the future of *the same signal at the same point along the spine*, whereas, here, we do the canonical correlation analysis of the past of *one signal* and the *time-shifted* future of *another signal at another point along the spine*. The previous analysis would yield an innovation model of the process at a single point, while the present one would yield a model of Y driven by X.

Remark: The linear canonical correlation analysis is, strictly speaking, relevant only to the case of Gaussian signals, which is a problematic assumption here[2]. The reason why we feel the linear canonical correlation analysis is adequate is that we observed that the nonlinear canonical correlation analysis produces only a moderate increase of the canonical correlation coefficients compared with the linear case [1]. Also the Alternating Conditional Expectation (ACE) modeling of the sEMG signal as $X(k+1) = \sum_{i=0}^{L-1} \phi_i(X(k+i))$ revealed regression functions ϕ_i fairly linear around 0 and then saturating [1].

2.2 Correlation among time-shifted phenomena at various points

A somewhat simplified approach is to compute the *scalar* correlation coefficient between the *random variables* $X(k), Y(k+T_s)$, rather than computing the canonical correlation *matrix* between the random vectors $X_-(k)$, $Y_+(k+T_s)$. The scalar correlation coefficient [4, p. 74] between the random variables $X(k)$ and $Y(k+T_s)$ is defined as

$$\rho(T_s) = \frac{E((X(k) - EX(k))(Y(k+T_s) - EY(k+T_s)))}{\sqrt{E(X(k) - EX(k))^2}\sqrt{E(Y(k+T_s) - EY(k+T_s))^2}}$$

This approach is statistically implemented as follows [4, Chap. 12]:

$$r(T_s) = \frac{\sum_{k=1}^{K-T_s} \left(X\left(k\right) - \bar{X}\left(T_s\right)\right)\left(Y\left(k+T_s\right) - \bar{Y}\left(T_s\right)\right)}{\sqrt{\sum_{k=1}^{K-T_s} \left(X\left(k\right) - \bar{X}\left(T_s\right)\right)^2}\sqrt{\sum_{k=T_s+1}^{K} \left(Y\left(k\right) - \bar{Y}\left(T_s\right)\right)^2}}$$

where

$$\begin{aligned} \bar{X}\left(T_s\right) &= \frac{1}{K-T_s} \sum_{k=1}^{K-T_s} X\left(k\right) \\ \bar{Y}\left(T_s\right) &= \frac{1}{K-T_s} \sum_{k=T_s+1}^{K} Y\left(k\right) \end{aligned}$$

[2]This assumption could be removed by bootstrapping.

Then the optimal time shift T_s^* is defined as the time shift that maximizes the absolute value of the correlation coefficient r.

Given that $r(T_s) \neq 0$, it is necessary to determine, with enough confidence, whether $\rho(T_s) \neq 0$, that is, whether there exists a *nonvanishing* correlation between $X(k)$ and $Y(k+T_s)$. This confidence analysis is based on the fact that, when $X(k), Y(k+T_s)$ are independently ($\rho = 0$) Gauss distributed, the variable

$$t = r\frac{\sqrt{K - T_s - 2}}{\sqrt{1 - r^2}}$$

approximately follows a t-distribution with $K - T_s - 2$ degrees of freedom [4]. [3] From this, a lower bound on $|t|$, hence on $|r|$, can be found such that $\rho \neq 0$ with a prescribed level of confidence.

Existence of a correlation between $X(k)$ and $Y(k + T_s)$ reveals a regression relation that could take either form

$$\begin{aligned} Y(k + T_s) &= aX(k) + b \\ X(k) &= a'Y(k + T_s) + b' \end{aligned}$$

Since $aa' = r^2$, the correlation does not assign a preference to either relation. Ultimately, what regression, if any, should be preferred depends on the behavior of $r(T_s)$ as a function of T_s. If $r(T_s)$ increases as T_s increases from 0, then the first one should be preferred, which indicates that X is the cause and Y is the effect. However, no such increase of $r(T_s)$ with T_s has been found, so that there is no objective preference for either regression. Specifically, $r(T_s)$ behaving as $\pm\cos\omega T_s$ on the subband signal indicates a stationary wave phenomenon.

2.2.1 raw signals

Taking the correlation between the total signals, without preprocessing, at two different points is straightforward, but the resulting correlation is a bit weak, does not show a very clear pattern, and as such is a bit hard to interpret. A way to increase the correlation is provided in the next section.

2.2.2 wavelet subband signals

Here, the idea is to first perform a wavelet decomposition of original time-series signals, eliminate those subbands that can be identified as noise, and then do the correlation analysis on those remaining subband signals that appear most relevant to the NSA wave.

The Daubechies wavelet of order 3 ("DB_3") appeared to be the most appropriate. This finding is fully consistent with [12], where DB_3 was also adopted, for the slightly different reason that this wavelet mimics the single Motor Unit Action Potential (MUAP) detected by the electrodes. Another reason why the

[3] Also recall that the sample distribution of $\frac{1}{2}\log\frac{1+r}{1-r}$ is approximately Gaussian with mean $\frac{1}{2}\log\frac{1+\rho}{1-\rho}$.

wavelet analysis works well is that the sEMG signal generated by NSA exhibits *some* self-similarity with a Hurst parameter between 0.51 and 0.55.

The signal was dyadic decomposed down to 8 levels as

$$\begin{aligned} X(k) &= D_1(k) + A_1(k) \\ X(k) &= D_1(k) + D_2(k) + A_2(k) \\ &\vdots \quad\quad \vdots \\ X(k) &= \sum_{i=1}^{7} D_i(k) + D_8(k) + A_8(k) \end{aligned}$$

where D stands for "details" (or high resolution) and A stands for "approximation" (or low resolution). More specifically, if $\{\psi_{mn}(k) = 2^{-m/2}\psi(2^{-m}k - n)\}$ denote the orthonormal wavelet with m the resolution and n the shift and ψ the Daubechies function, the signal has representation

$$X(k) = \sum_{m,n} c_{mn}\psi_{mn}(k)$$

and the above decomposition reads:

$$\begin{aligned} X(k) &= \sum_{n} c_{1n}\psi_{1n}(k) + \sum_{m>1}\sum_{n} c_{mn}\psi_{mn}(k) \\ X(k) &= D_1(k) + \sum_{n} c_{2n}\psi_{2n}(k) + \sum_{m>2}\sum_{n} c_{mn}\psi_{mn}(k) \\ &\vdots \quad\quad \vdots \\ X(k) &= \sum_{i=1}^{7} D_i(k) + \sum_{n} c_{8n}\psi_{8n}(k) + \sum_{m>8}\sum_{n} c_{mn}\psi_{mn}(k) \end{aligned}$$

It turns out that the D_8 subband signal has very good correlation properties. To understand its spatial correlation properties, we write it as

$$u(x,k) = \sum_{n} c_{8,n}(x)\psi_{8,n}(k)$$

Clearly, the $c_{8,n}$ coefficients are patient specific. From the above decomposition, the computed correlation is

$$\frac{\overline{u(x_1,k)u(x_2,k+T_s)}}{||u(x_1,\cdot)|| \cdot ||u(x_2,\cdot)||} = \sum_{n_1,n_2} \frac{c_{8,n_1}(x_1)c_{8,n_2}(x_2)}{\sqrt{\sum_{n_1} c_{8,n_1}^2(x_1) \sum_{n_2} c_{8,n_2}^2(x_2)}} \overline{\psi_{8,n_1}(k)\psi_{8,n_2}(k+T_s)} \tag{1}$$

Clearly, this correlation has a patient specific component, because of the first factor in the right hand side, but it also has a wavelet specific component,

because of the second factor in the right hand side. Now remember that n_2 is a delay which combines with T_s, so that by orthogonality the double sum reduces to a sum along a parallel to the diagonal, viz., $n_2 + 2^{-m}T_s = n_1$, so that the above reduces to

$$\frac{\overline{u(x_1,k)u(x_2,k+T_s)}}{||u(x_1,\cdot)|| \cdot ||u(x_2,\cdot)||} = \sum_{n_1} \frac{c_{8,n_1}(x_1)c_{8,n_1-2^{-m}T_s}(x_2)}{\sqrt{\sum_{n_1} c^2_{8,n_1}(x_1) \sum_{n_2} c^2_{8,n_2}(x_2)}} \tag{2}$$

3 data collection

To record sEMG signals, ungelled, noninvasive electrodes were placed at cervical, thoracic, lumbar, and sacral positions along the spine. The unfiltered sEMG data was collected over a bandwidth of 10-500 Hz by an Insight^{TM} Millennium machine, converted to digital format with a 16 bit precision DAS16/16 PCMCIA card, and stored on a PC compatible laptop computer. FFT analysis of the signals revealed a peak at about 125 cycles/sec.

The data used here was collected in two different sessions:

1. S99: An older recording session in 1999, at a sampling frequency of 2000 samples/sec., using a baseline subject BL99.

2. S04: A recent recording session in 2004, at a sampling frequency of 4000 samples/sec., using a baseline subject BL04 and a quadriplegic subject Q04. The latter subject had a swimming pool accident, dove in deep end of pool with only 4 feet of water, sustained C-5 spinal cord injury (similar to the case reported in [9]), C-5 vertebrae was surgically removed and replaced with a titanium plate from C-4 to C-6.

All research subjects had previously signed the *Informed Consent Form* in a protocol approved by the Institutional Review Board (IRB) of the University of Southern California.

In order to assess noise or other irrelevant pattern during S04, before entrainment but with the research subject in the same position and with the same wiring as during entrainment, time-series signals were recorded to be used as control or testing signals. Then, keeping the same experimental environment, the subject was entrained and the NSA wave was recorded. This protocol was used for both BL04 and Q04.

The "lag" L was systematically set to 25.

4 spatio-temporal analysis of collected signals

4.1 canonical correlation analysis of sEMG signals

The relationship between the time shift T_s and the past/future mutual information for the research subject BL99 (Level 2) was derived via canonical correlation

analysis. The results when X is the sacral signal and Y the lumbar, thoracic, and cervical signal are shown in Figure 1-4, respectively.

The mutual information between the sacrum signal X and the other signals Y is a function of T_s, first increasing, then reaching a maximum for $T_s > 0$, and then decreasing. More specifically, from Figures 1 and 3, it appears that the electrophysiological phenomenon takes 30 sample points (15 msec.) to travel from the sacrum to the neck and 10-20 sample points (5-10 msec.) to travel from the sacrum to the lumbar spine, respectively. (A problem is that Figure 2 indicates that the wave takes 6 sample points (3 msec.) to go from the sacrum to the thorax, which is hard to reconcile with the previous traveling times, unless there exists some more direct nervous pathway from the sacrum to the thorax?) Putting on the side the thorax data, this analysis indicates that the sacrum area is the excitation, or the source of the wave, and that the lumbar, thoracic, and cervical signals are delayed versions of the sacral signal, therefore establishing a traveling wave pattern from the sacrum to the neck. That the sacrum is the excitation, or the cause, should not come too much as a surprise, since at the sacrum the filum terminale of the distal end of the spinal cord is attached to the bony structure of the coccyx.

Observe that the above traveling wave analysis reveals a electrophysiological propagation speed of roughly 100 m/sec., which is consistent with accepted figures [14, p. 59].

4.2 correlation analysis of sEMG phenomena

4.2.1 raw sEMG data signal

For BL04, the computed correlation coefficients between random variables at various points and for various time-shifts are shown in the plots of Figures 5-8.

First, the correlation between the sEMG random variable at a point and the time-shifted random variable *at the same point* is relevant to the dynamics of this signal at that point and shows a nonsurprising oscillatory behavior.

When it comes to the correlation between *two different points*, we can already perceive a pattern: Across Figures 5-8, observe that, for $T_s = 0$, there is opposite phase between, on the one hand, the neck random variable and, on the other hand, the thorax, lumbar spine, and sacrum random variables.

4.2.2 wavelet subband sEMG signal

In order to exhibit better correlation (hence higher confidence) and a more coherent phase pattern, we basically redo the same analysis but on the D_8 subband signal.

For both research subjects BL04 and Q04, all control and NSA signals were dyadic decomposed down to 8 levels with the Daubechies wavelet function [6, 13, 5] of order 3. By comparing the control and NSA wave signals (see Fig. 9), it becomes evident that the signals in A_8 are just base line drifting or low frequency noises (long term evolution) and as such are signals of no interest;

neither are the signals in the D_1 to D_5 subbands of interest, because there is no difference between the test and the NSA signals and as such these signals consists mainly of high frequency noise. On the other hand, it is evident that the D_6, D_7, D_8 components are of more interest, because there is now a sizable difference between the test and NSA signals. Also, observe the marked "wavelet packets" in the D_7, D_8 subband signals, which are bursting phenomena running up and down the spine and establishing a "stationary" wave pattern. While a correlation analysis on D_7 could be carried out, we selected the D_8 signal, because it showed the better correlation properties.

The confidence level was set to 99%, meaning that the correlation is significant whenever the $r(T_s)$ versus T_s curve is outside the horizontal band bounded by the two lines parallel to the T_s axis. The time delay between each signals is around 100-150 samples points.

baseline subject (BL04)

The results of the correlation analysis of the D_8 subband signals for various time-shifts are shown in the plots of Figures 10-13. Observe that the curves are well outside the "slit" along the T_s axis, indicating a 99% confidence in the correlation.

Most importantly, observe the consistent phase pattern, with "zero crossing nodes," much more pronounced than in the previous approach. (A "zero crossing node" is defined as a point where all four $r(T_s)$ versus T_s curves cross the $r = 0$ axis.)

If, in Equation 2, we set $x_1 = x_2 = x$, then the correlation becomes

$$r(T_s) = \frac{\sum_n c_{8,n}(x) c_{8,n-2^{-m}T_s}(x)}{\sum_n c_{8,n}^2(x)}$$

which vanishes for $T_s = 40$ samples points, etc. This gives an indication of *the frequency of the oscillation at the point x, or at any other point along the spine for that matter.*

Next, setting $T_s = 0$ in Equation 2 yields

$$r(T_s) = \frac{\sum_n c_{8,n}(x_1) c_{8,n}(x_2)}{\sqrt{\sum_{n_1} c_{8,n_1}^2(x_1) \sum_{n_2} c_{8,n_2}^2(x_2)}}$$

which obviously from the diagrams changes sign. Therefore, there exists at least one point x_* where the above vanishes, viz.,

$$\sum_n c_{8,n}(x_*) c_{8,n}(x_*) = ||c_{8,\cdot}(x_*)||^2 = 0$$

which indicates existence of a *mode shape node* at x_*. Clearly, there exists such a node somewhere between the neck electrode and the thoracic electrode. We further conjecture that there are no waveform nodes between the thorax and the sacrum, because changes in the waveform signs between the thorax and the sacrum appear inconsistent with the kinematics of the spine. That there exists

a waveform node between the neck electrode and the thorax electrode can be justified by the kinematic flexibility of the neck.

Clearly, all of the above indicates a stationary wave phenomenon.

quadriplegic subject (Q04)

The same correlation analysis, but on the quadriplegic subject Q04, is shown in Figures 14-17.

First, observe that all correlations involving the neck signals are weak, as can be anticipated from the neck injury, *but they are still in the 99% confidence interval. This positive correlation between signals on both sides of the spinal cord injury indicates that nerve impulses pass through, or peripherally around, the injury area, hence indicating some partial motor recovery.*

Second, the stationary wave pattern does not appear as clearly as for the baseline subject, as can be seen by the defective "zero crossing nodes." However, the thoracic, lumbar, and sacral plots (Fig. 15, 16, 17, resp.) do show zero crossing nodes, *if we remove the neck signals from those plots. It therefore appear that there is some stationary pattern involving the thorax, lumbar spine, and sacrum, but not involving the neck.*

In conclusion, it appears that the stationary wave pattern cannot completely establish itself, because of the neck injury.

comparison

To allow for an easy comparison between the baseline and quadriplegic subjects, the correlation curves of Fig. 10-17 are merged into Fig. 18, with the baseline subject curves on the left and the quadriplegic subject curves on the right. The first and most striking difference between the baseline subject (Fig 10) and the quadriplegic subject (Fig 14) is a weaker correlation between, on the one hand, the neck and, on the other hand, the cervical, thoracic, lumbar or sacral signals, as can be anticipated because of the neck injury. Another striking difference is that, in the thoracic, lumbar and sacral plots of Fig. 18, the correlation involving the neck signal of the quadriplegic subject is off phase as compared with the baseline subject. While there is considerable debate as to whether and how regeneration occurs, this extra phase shift seems to indicate that the regeneration has happened via the periphery of the cord.

5 Conclusions

Using statistical correlation techniques on the sEMG signals recorded at various points along the paraspinal muscles, the Network Spinal Analysis (NSA) wave phenomenon has been positively identified and, on a baseline subject, has been shown to take the form of a stationary wave. As shown more specifically in this paper, it appears necessary to restrict the correlation to a selected subband signal of the dyadic wavelet decomposition in order get a higher correlation and hence a test of significance of the nonvanishing correlation.

The NSA wave provides the same kind of repetitive motion that, as shown in [9], has already allowed late partial sensory and motor recovery from cervical spinal cord injury. As shown in this paper, the spatio-temporal wave analysis

developed here appears to be of help to assess this recovery. In particular, here, existence of a correlation between such distant signals as the cervical and sacral appears to indicate some spinal injury recovery. But some follow up on this patient is needed to positively assert this.

Acknowledgment

Many thanks to Dr. D. Epstein, Dr. R. Boone, Dr. L. Stern, and Mr. V. Mahajan for many helpful discussions.

References

[1] S. Bohacek and E. A. Jonckheere. Chaotic modeling in network spinal analysis: Preliminary report: Nonlinear canonical correlation with alternating conditional expectation (ACE). *Journal of Vertebral Subluxation Research*, 2(4):188–195, December 1998.

[2] A. Breig. *Adverse Mechanical Tension in the Central Nervous System*. John Wiley and Sons, New York, 1987.

[3] A. Breig. *Skull Traction and Cervical Cord Injury: A New Approach to Improved Rehabilitation*. Springer Verlag, 1989. ISBN: 0387504141.

[4] M. G. Bulmer. *Principles of Statistics*. Dover, New York, 1979.

[5] I. Daubechies. Orthonormal bases of compactly supported wavelets. *Communications on Pure and Applied Mathematics*, XLI:909–996, 1988.

[6] I. Daubechies. *Ten lectures on wavelets*. CBMS-NSF Conference Series in Appplied Mathematics. SIAM, 1992.

[7] Edmond A. Jonckheere and Poonsuk Lohsoonthorn. Dynamic modeling of surface electromyographic activity during various spinal conditions. In *American Control Conference (ACC2003)*, pages 465–470, Denver, CO, June 4-6 2003.

[8] P. Lohsoonthorn and E. A. Jonckheere. Nonlinear switching dynamics in surface electromyography of the spine. In *Physics and Control*, pages 277–282, St. Petersbourg, Russia, August 21-23 2003.

[9] J. W. McDonald, D. Becker, C. Sadowsky, J. A. Jane, T. E. Conturo, and L. Schultz. Late recovery following spinal cord injury. *J. Neurosurg (Spine 2)*, 97:252–265, 2002.

[10] M. Panjabi. The stabilizing system of the spine. part i. function, dysfunction, adaptation, and enhancement. *Journal of Spinal Disorders*, 5(4):383–389, 1992.

[11] E. E. Selkurt. *Physiology.* Little, Brown and Company, Boston, 1971.

[12] W.M. Sloboda and V.M. Zatsiorsky. Wavelet analysis of emg signals. In *Twenty-First Annual Meeting of the American Society of Biomechanics*, Clemson University, South Carolina, September 24-27 1997.

[13] G. Strang and T. Nguyen. *Wavelets and Filter Banks.* Wellesley-Cambridge, 1996.

[14] R. F. Thompson. *The Brain.* W. H. Freeman, New York, 1993.

[15] R. Warick and P. L. Williams, editors. *Gray's Anatomy.* W.B. Saunders Co., Philadelphia, 1973. 35th British Ed.

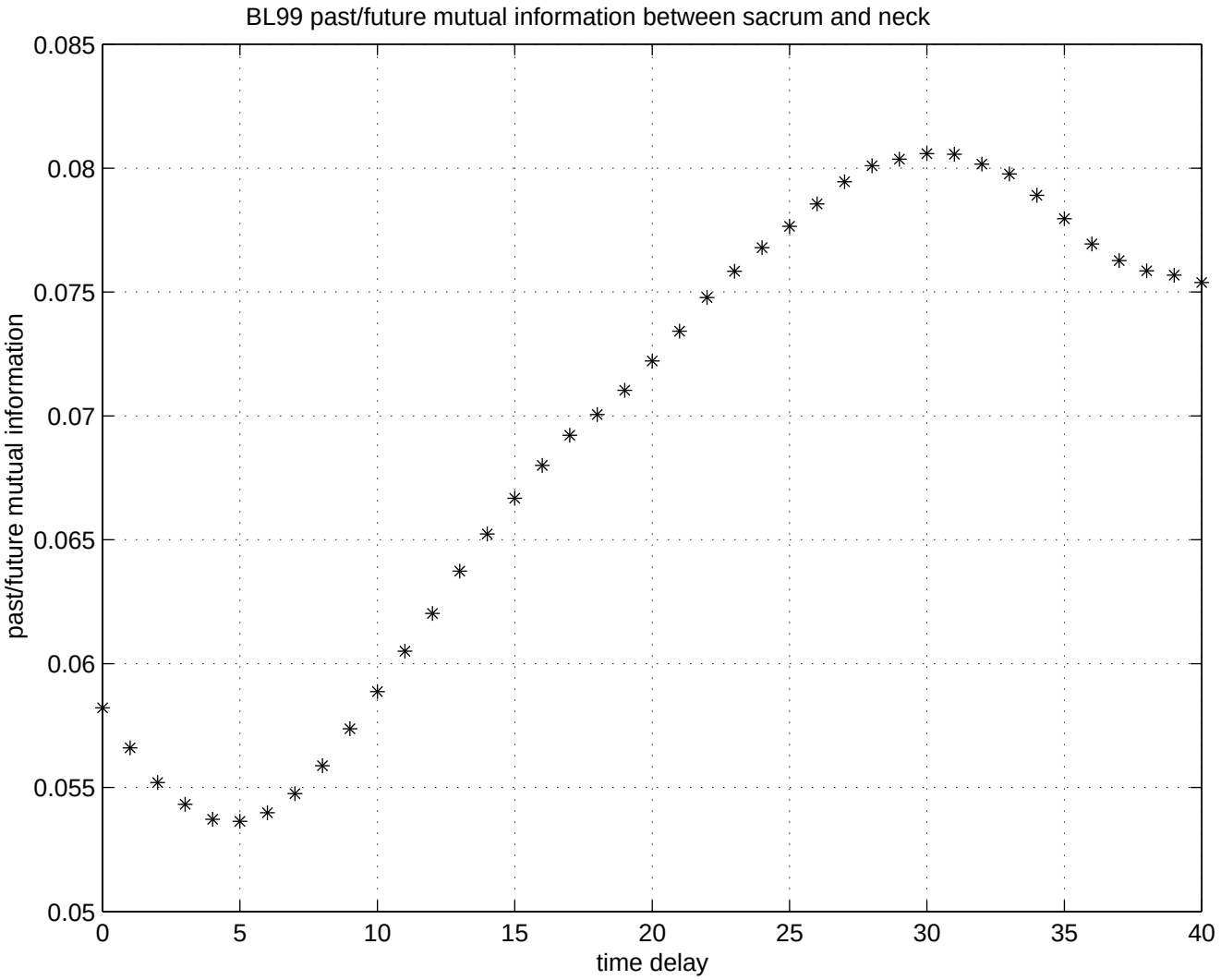

Figure 1: Mutual sacrum/neck information versus time-shift. Because the information reaches a maximum for $T_s > 0$, this plot establishes a traveling wave from the sacrum to the neck.

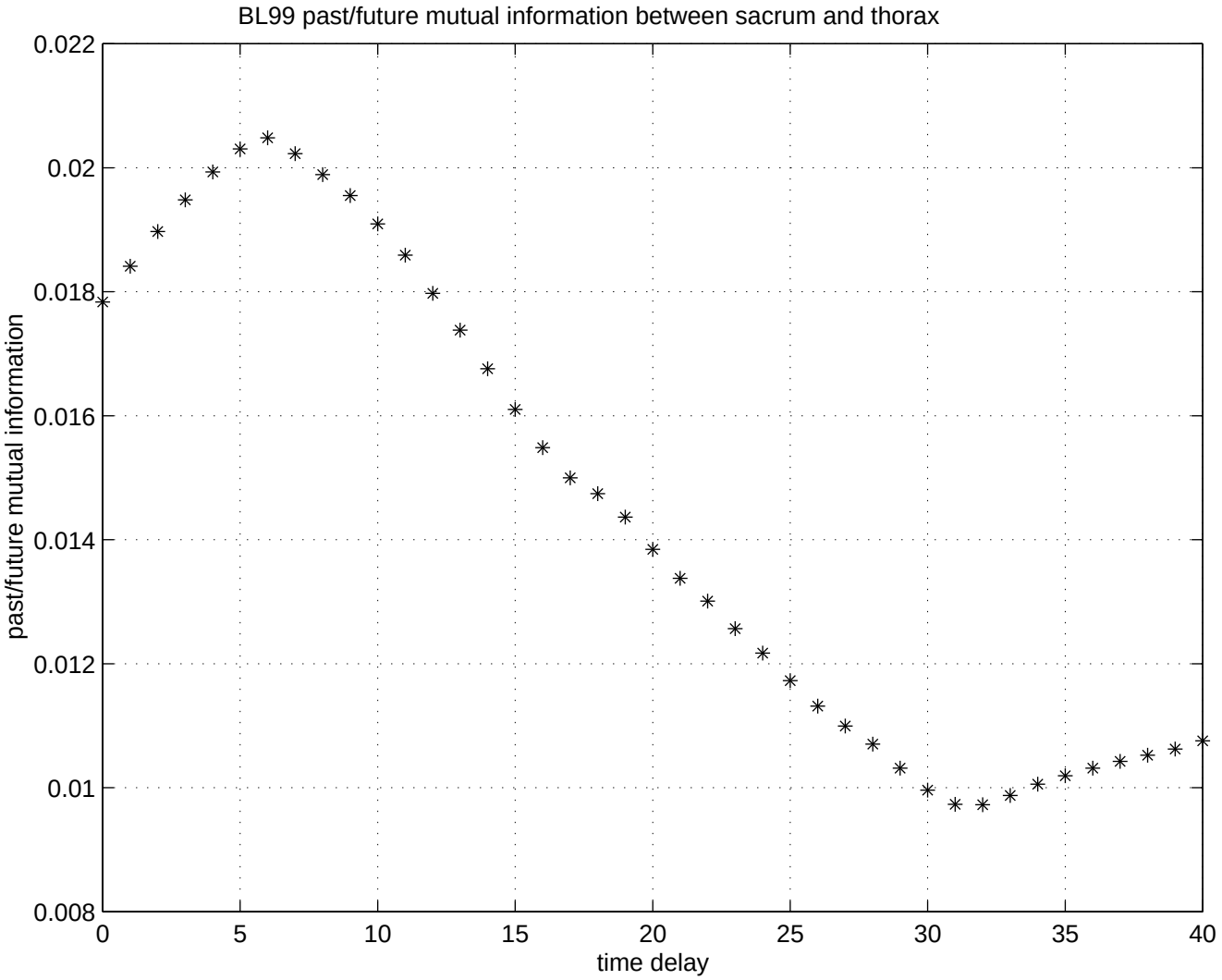

Figure 2: Mutual sacrum/thorax information versus time-shift. The fact that the information reaches a maxiumum for a small $T_s > 0$ seems (?) to reveal a fast traveling wave from the sacrum to the thorax.

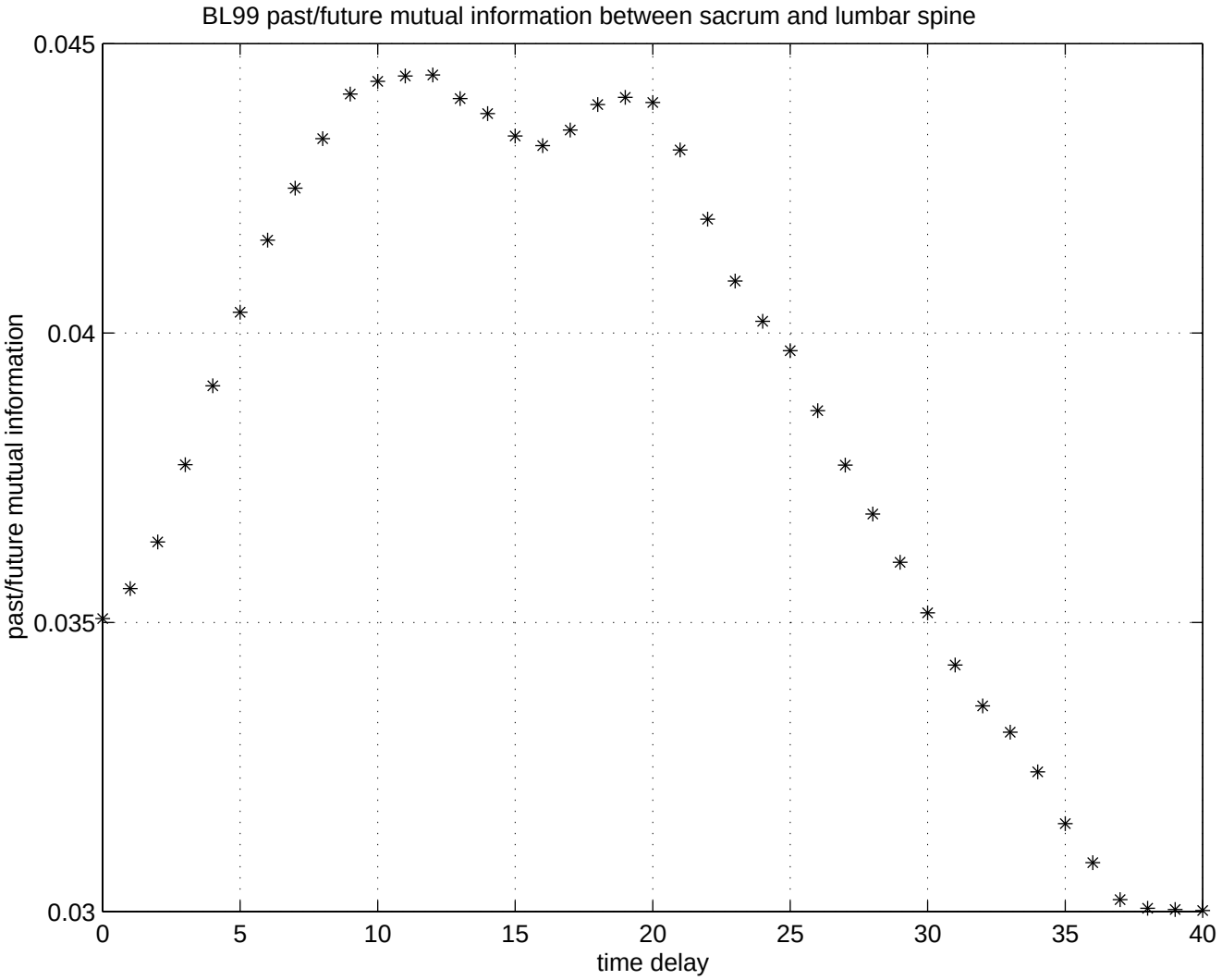

Figure 3: Mutual sacrum/lumbar spine information versus time-shift. Since the information reaches a maximum for $T_s > 0$, a traveling wave from the sacrum to the lumbar spine is established.

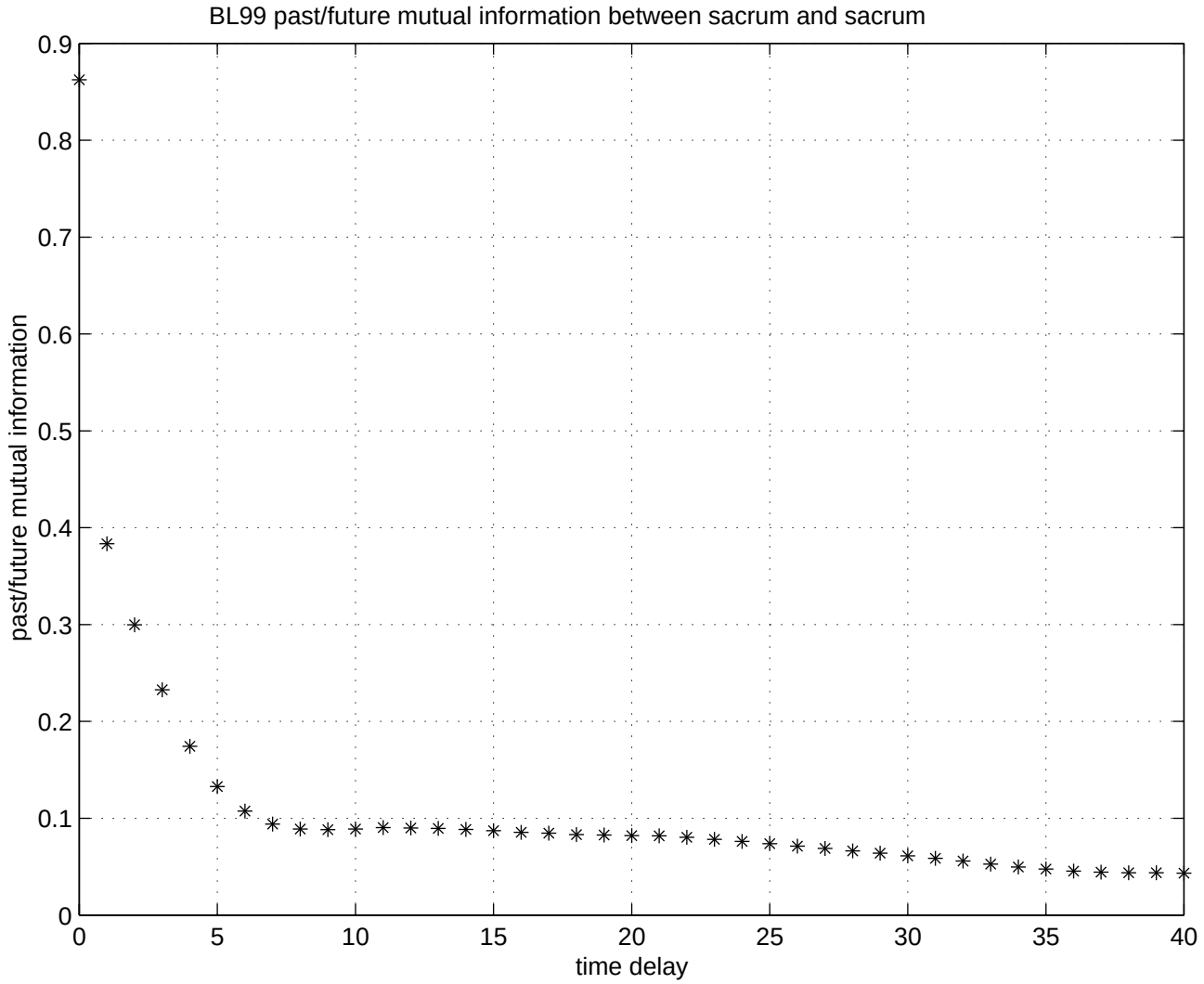

Figure 4: Mutual sacrum past/future information versus time-shift. Observe that the information is maximum for $T_s = 0$.

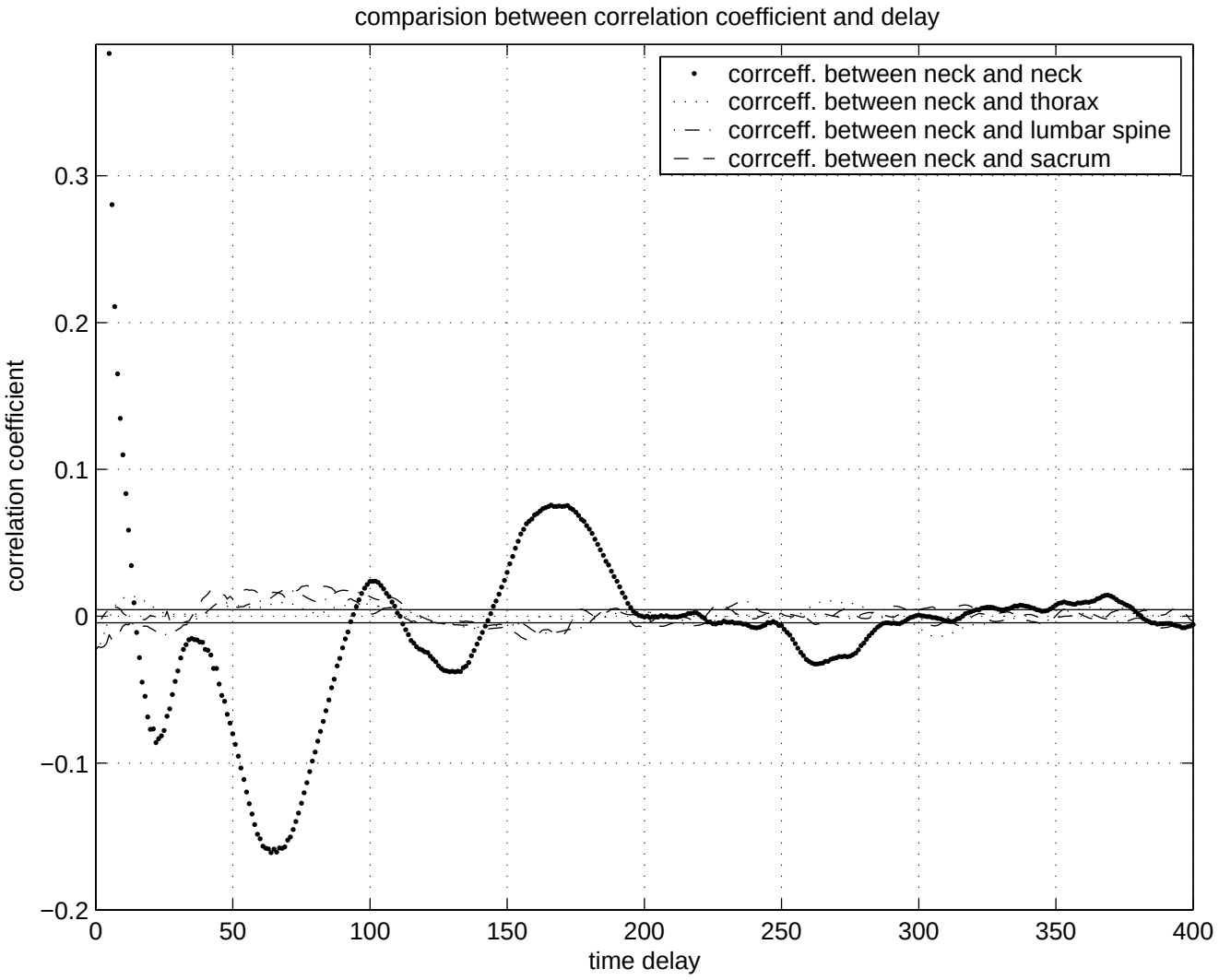

Figure 5: Correlation between neck and other signals for baseline subject BL04.

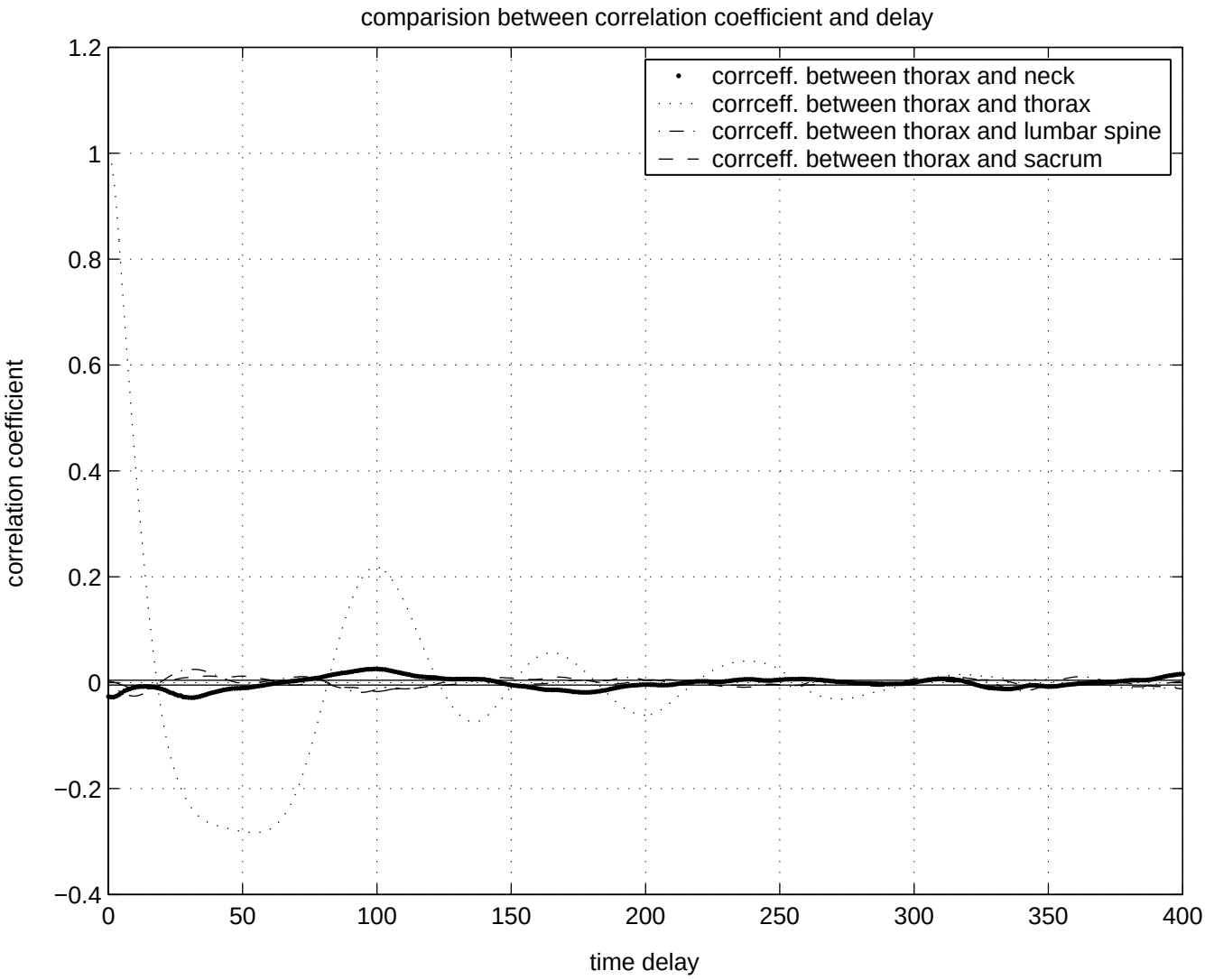

Figure 6: Correlation between thorax and other signals for baseline subject BL04.

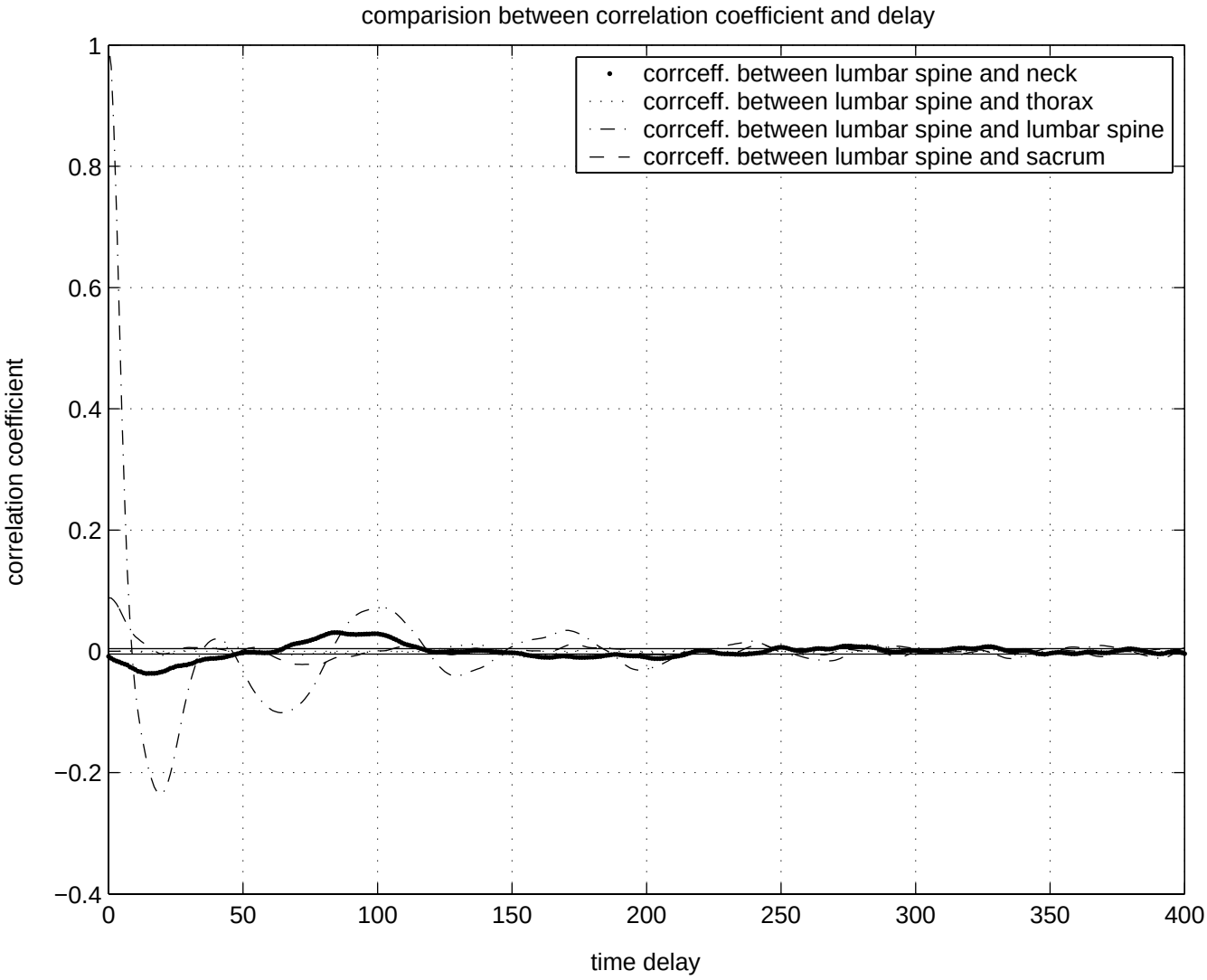

Figure 7: Correlation between lumbar spine and other signals for baseline subject BL04.

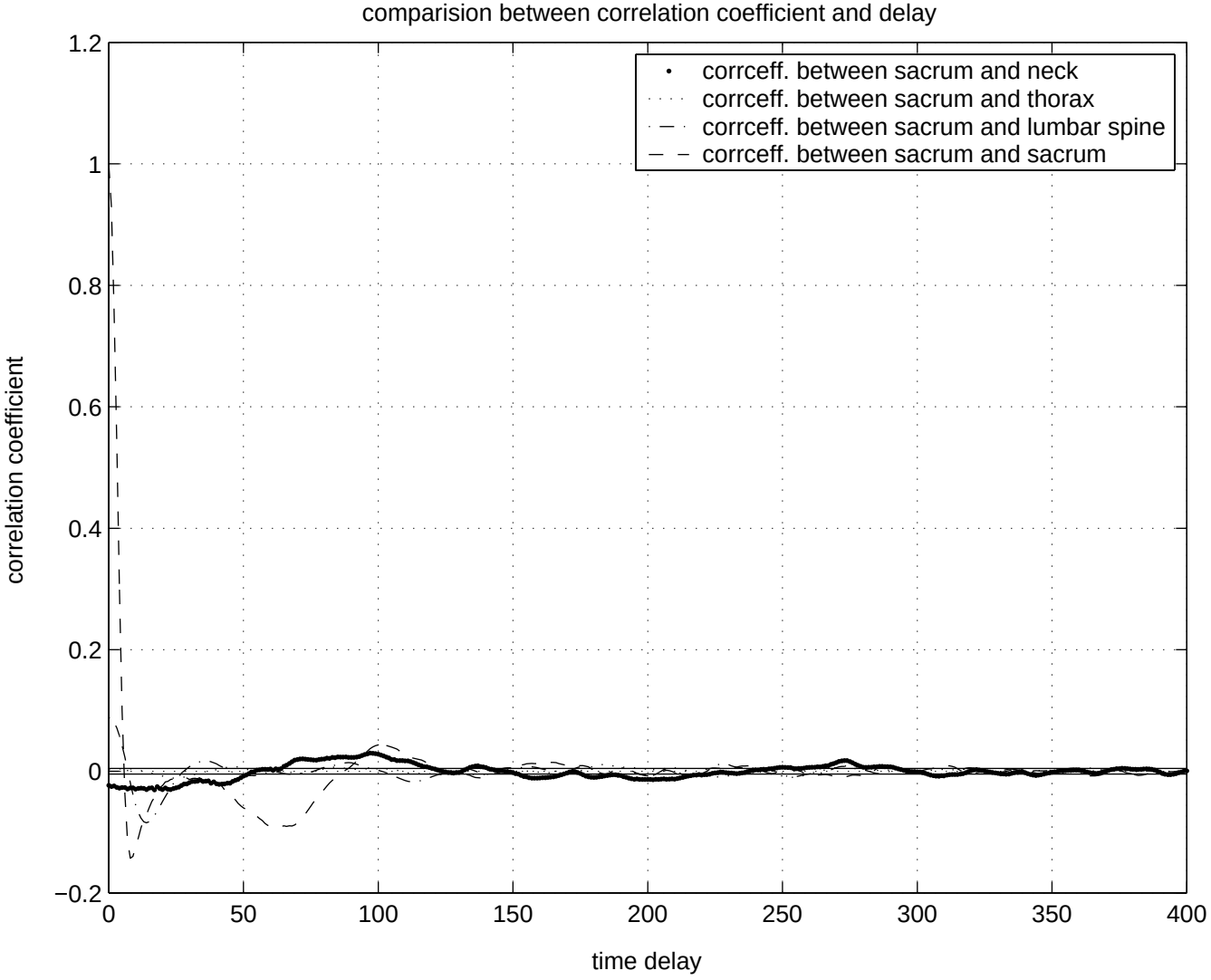

Figure 8: Correlation between sacral and other signals for baseline subject BL04.

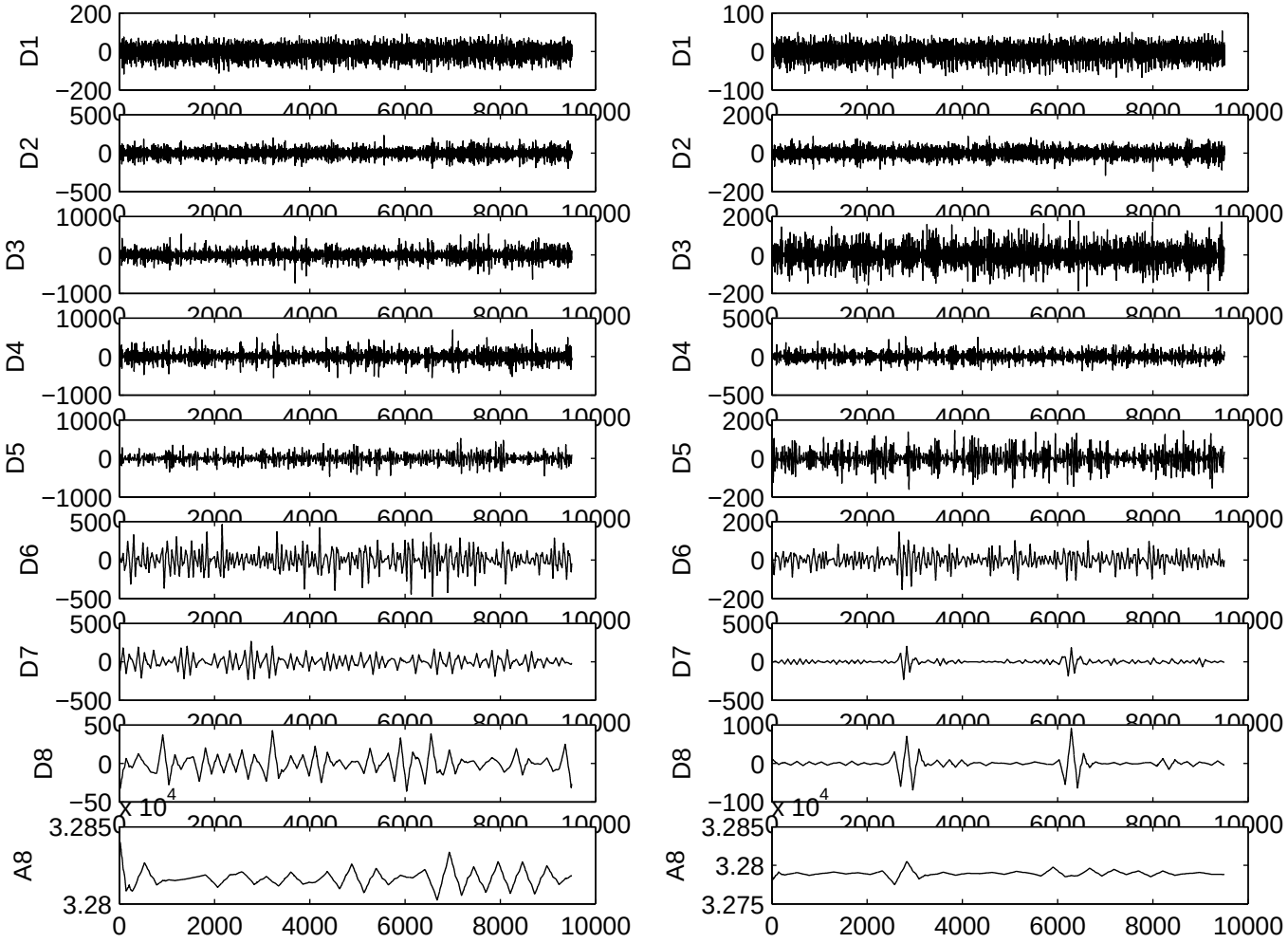

Figure 9: Comparison between wavelet decompositions of control signal (left) and NSA signal (right).

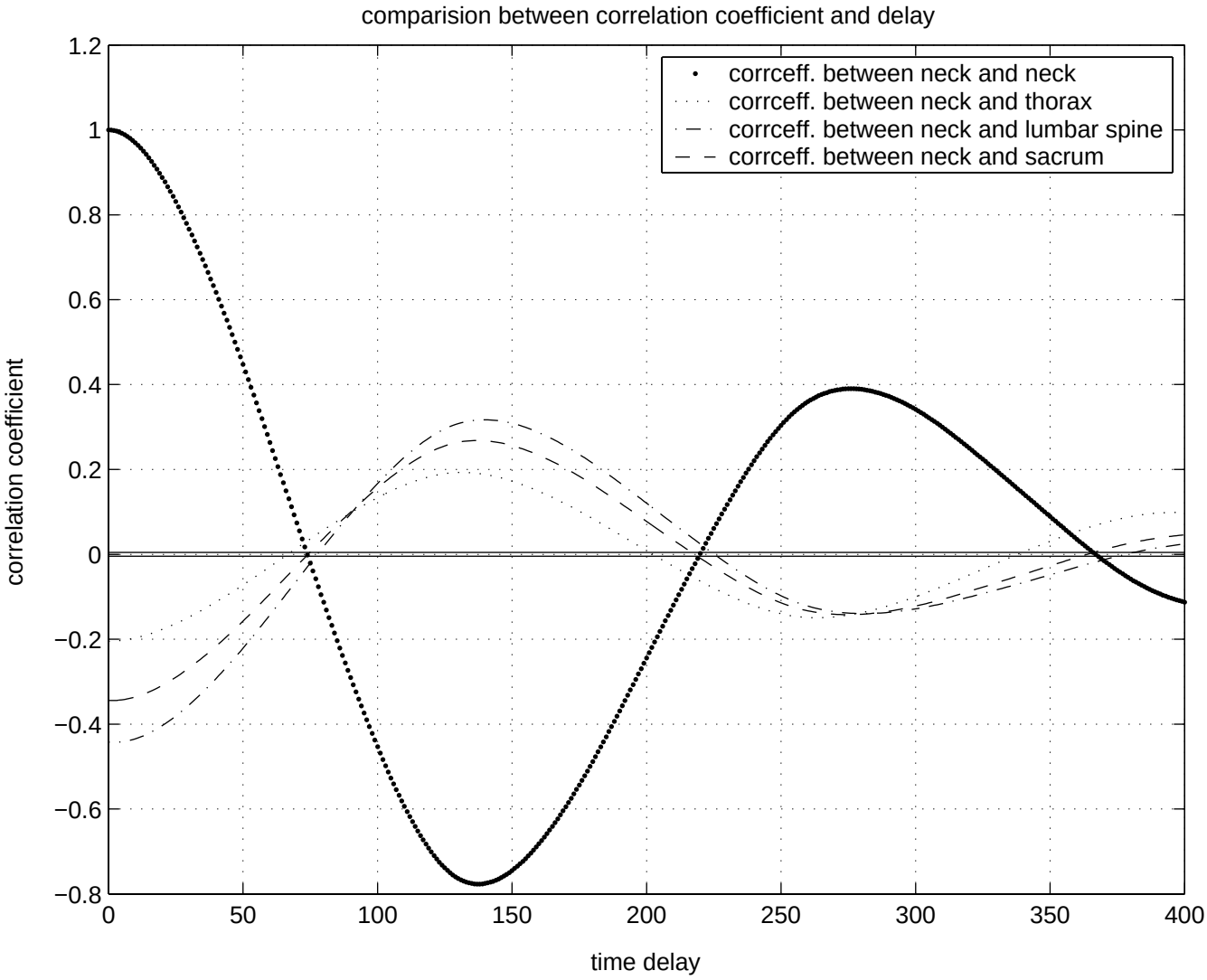

Figure 10: Correlation between subbands of neck and other signals for baseline subject BL04.

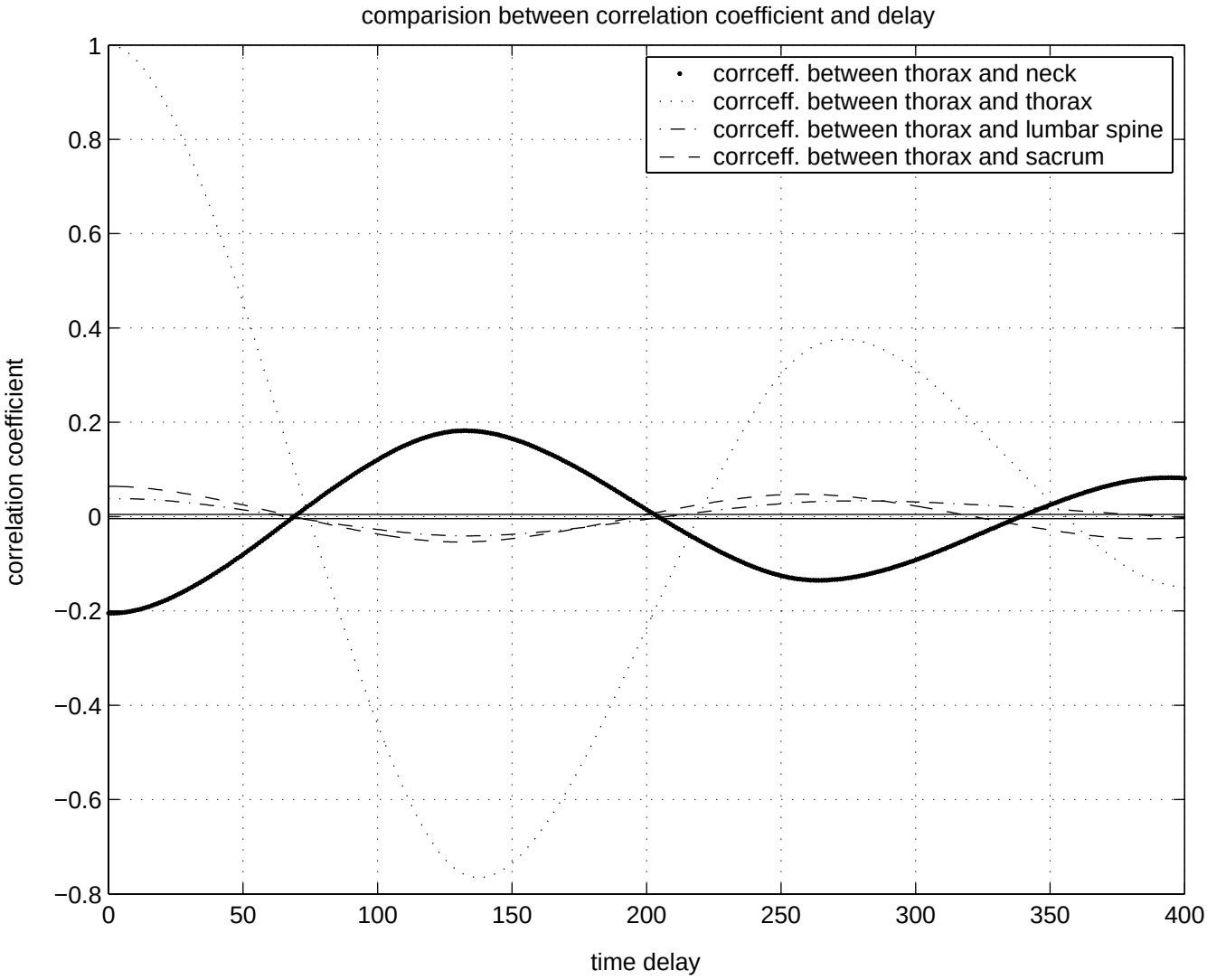

Figure 11: Correlation between subbands of thorax and other signals for baseline subject BL04.

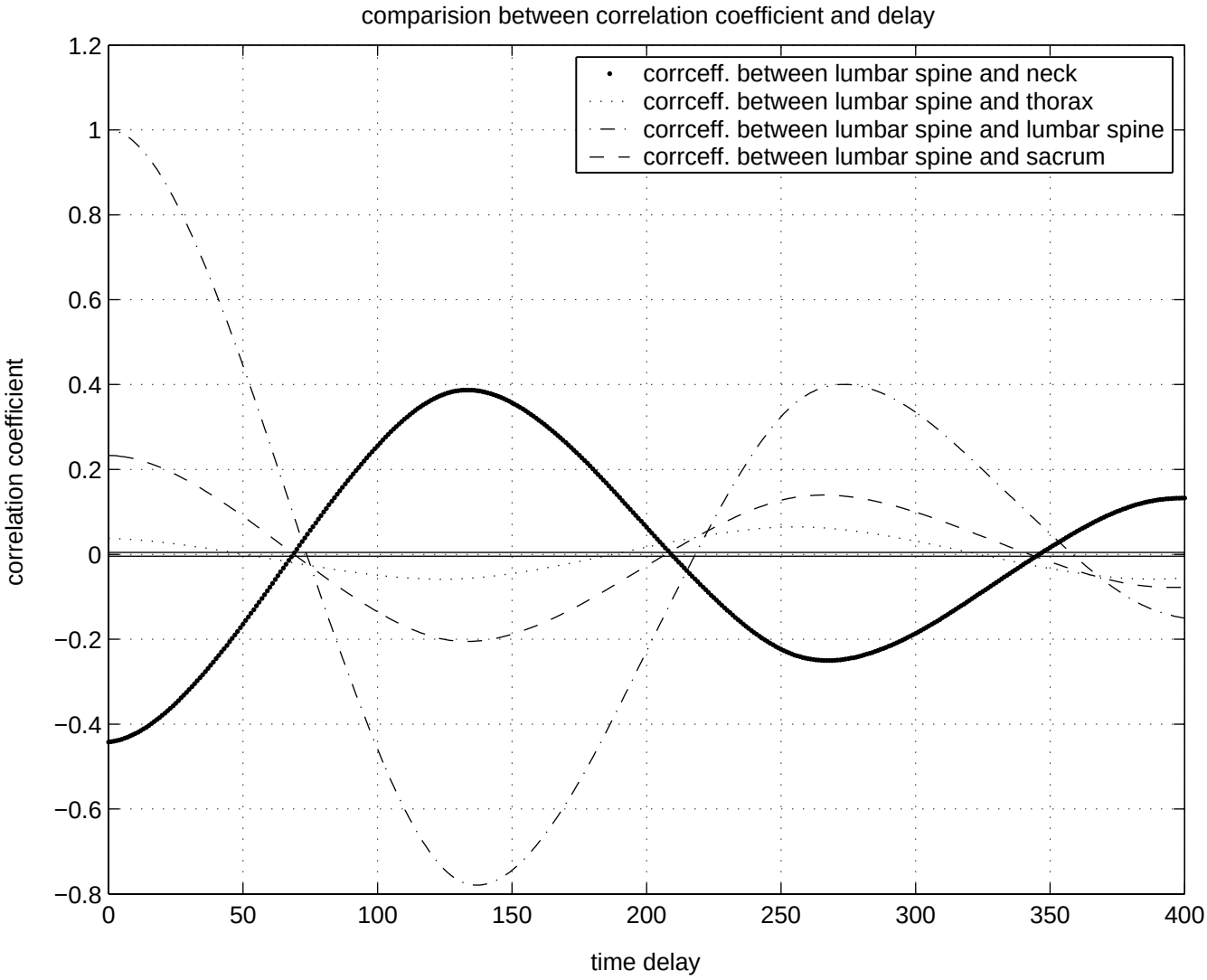

Figure 12: Correlation between subbands of lumbar spine and other signals for baseline subject BL04.

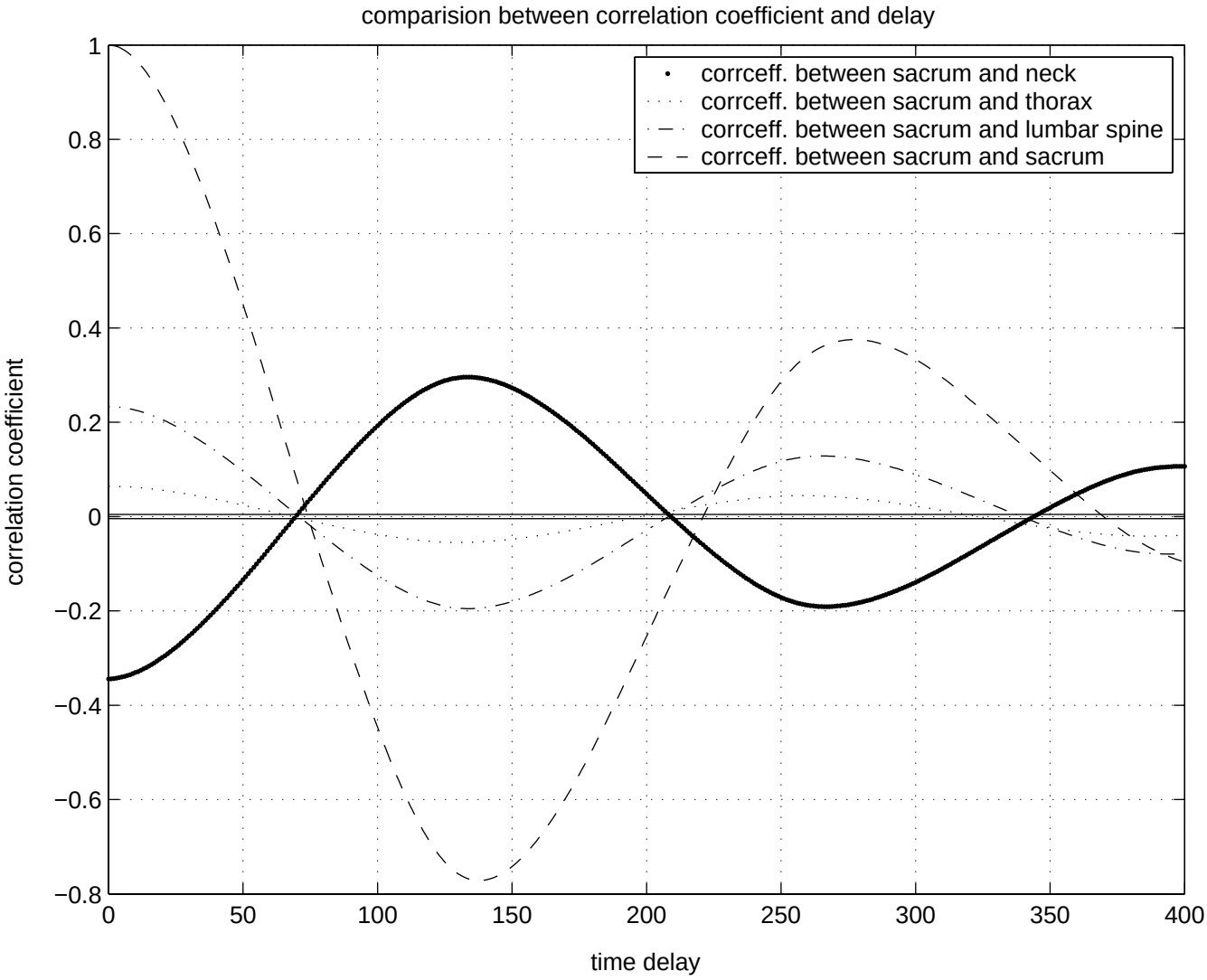

Figure 13: Correlation between subbands of sacrum and other signals for baseline subject BL04.

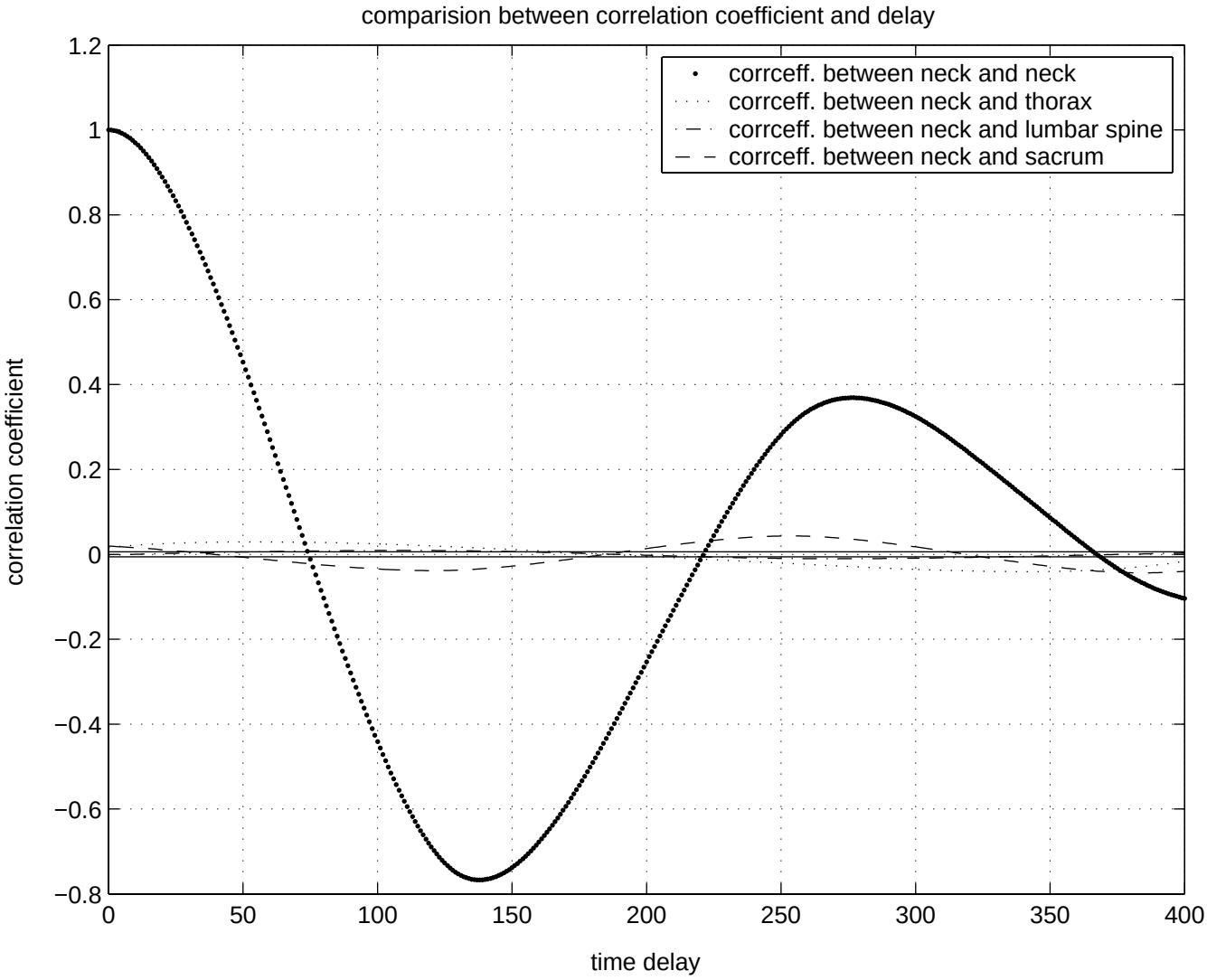

Figure 14: Correlation between subbands of neck and other signals for quadriplegic subject Q04.

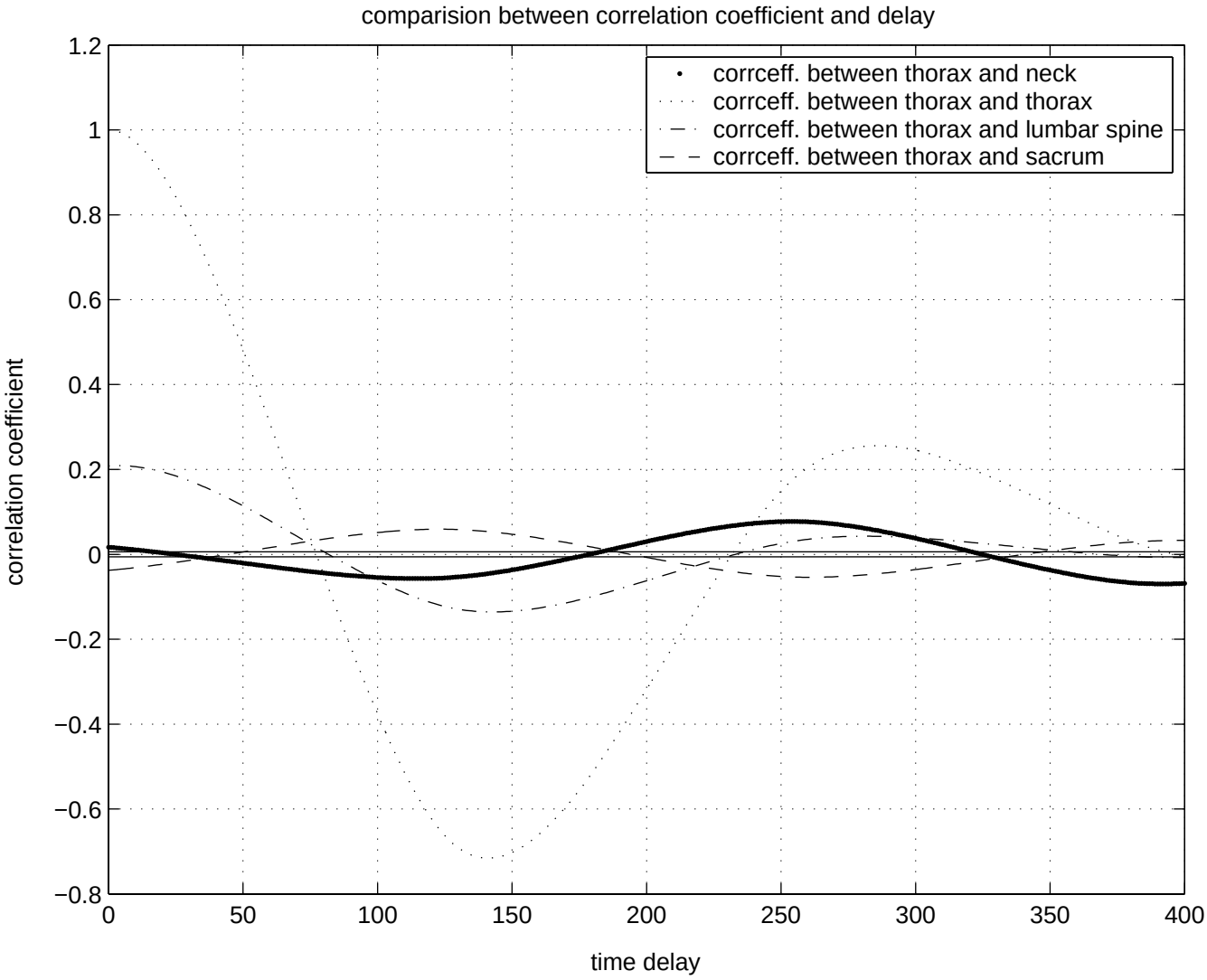

Figure 15: Correlation between subbands of thorax and other signals for quadriplegic subject Q04.

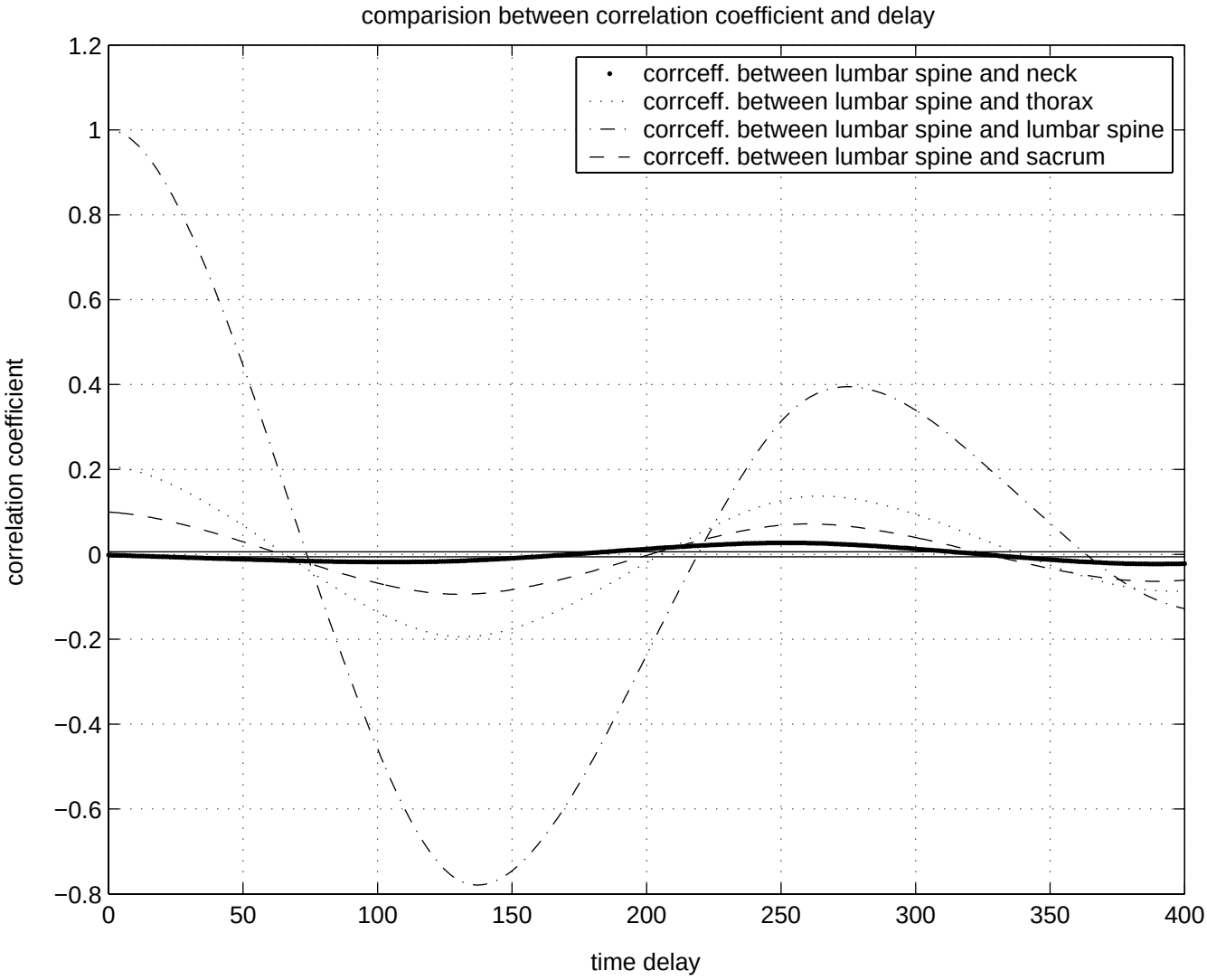

Figure 16: Correlation between subbands of lumbar spine and other signals for quadriplegic subject Q04.

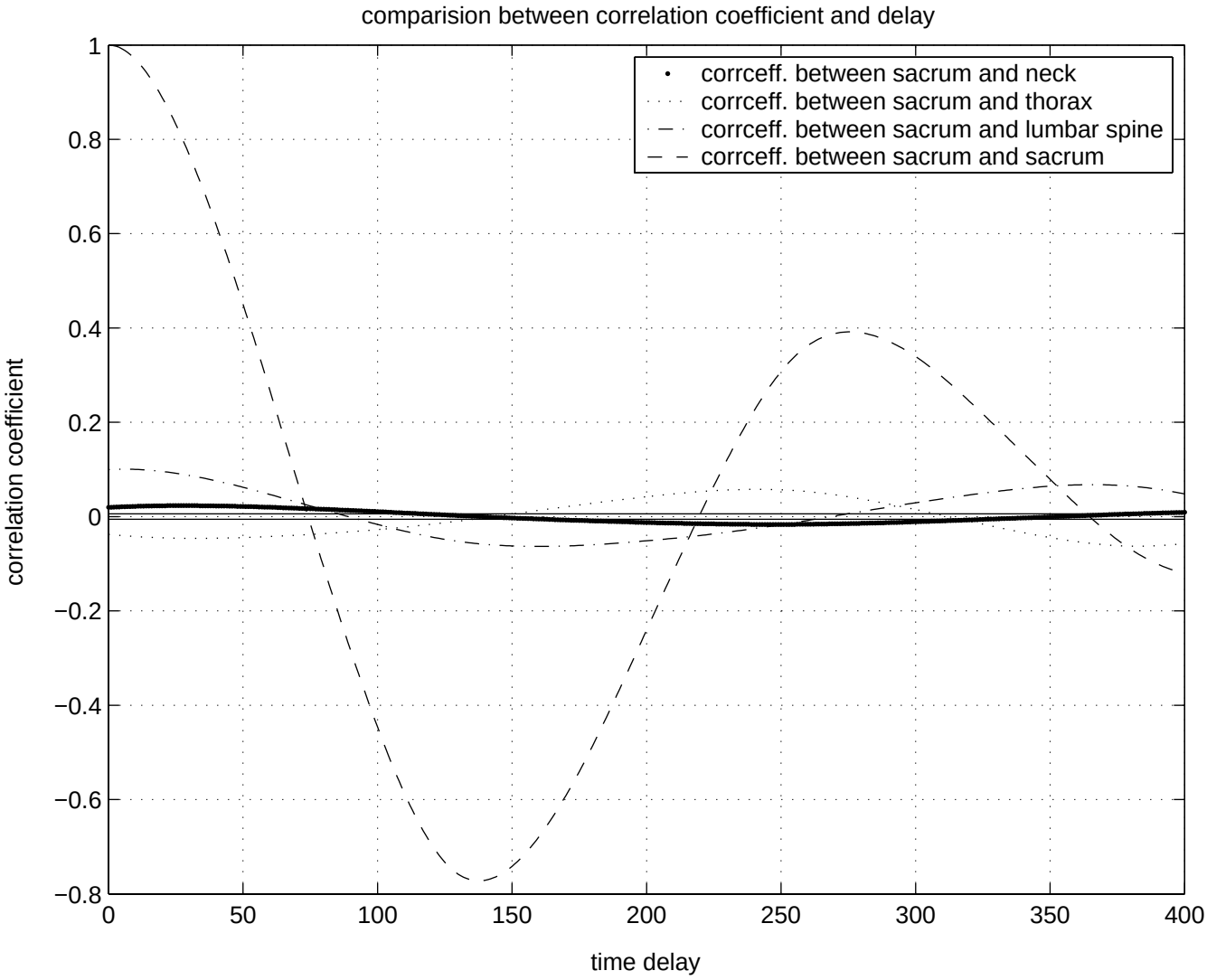

Figure 17: Correlation between subbands of sacrum and other signals for quadriplegic subject Q04.

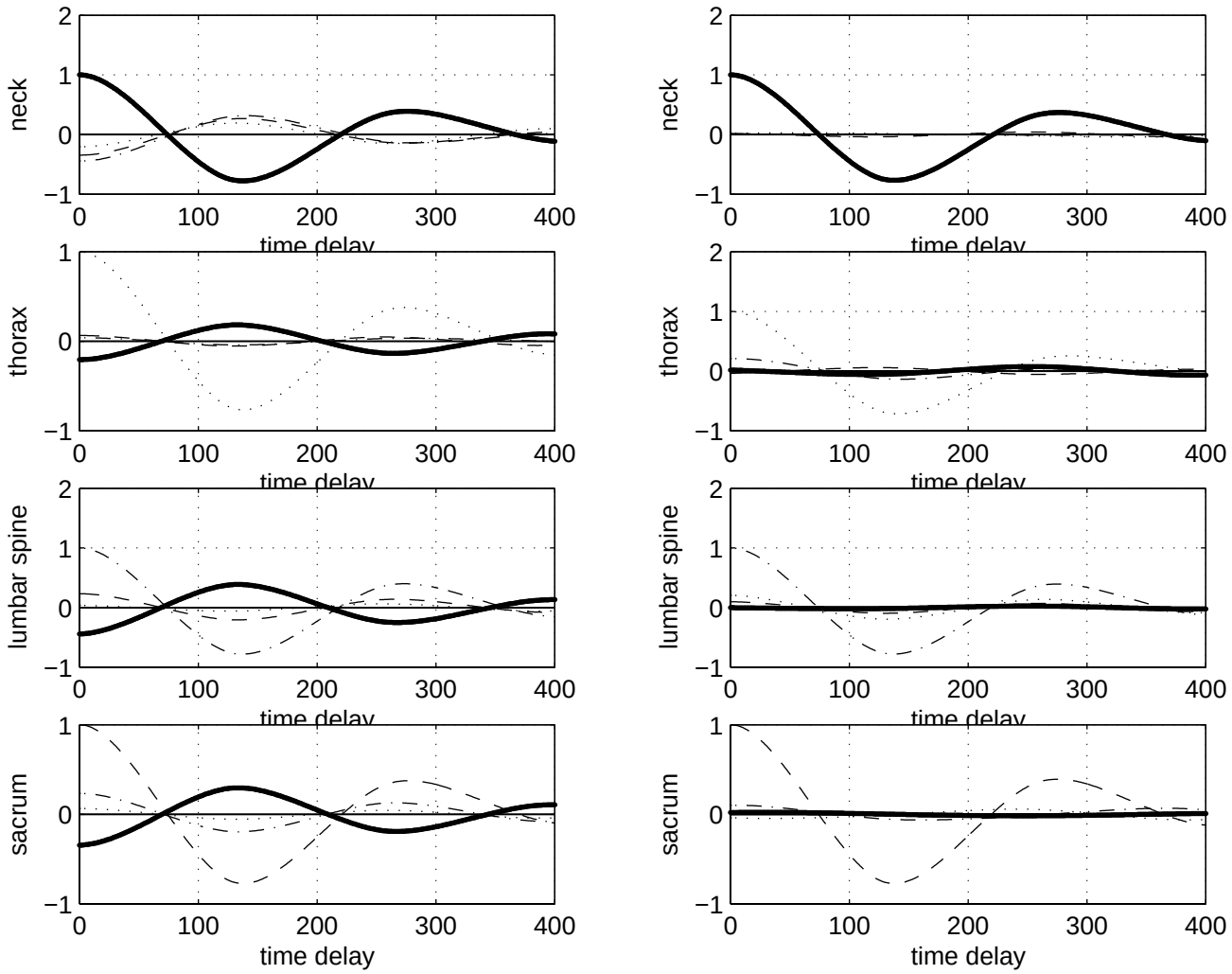

Figure 18: Comparison between correlation curves of baseline (left) and quadriplegic (right) subjects.